This article was downloaded by: [University of California, Berkeley]

On: 17 December 2013, At: 17:04

Publisher: Taylor & Francis

Informa Ltd Registered in England and Wales Registered Number: 1072954 Registered office: Mortimer House,

37-41 Mortimer Street, London W1T 3JH, UK



Journal of Modern Optics

Publication details, including instructions for authors and subscription information: http://www.tandfonline.com/loi/tmop20

Intensity dependence of light-induced states in transient absorption of laser-dressed helium measured with isolated attosecond pulses

M. Justine Bell^a, Annelise R. Beck^a, Hiroki Mashiko^a, Daniel M. Neumark^a & Stephen R. Leone^{ab}

To cite this article: M. Justine Bell, Annelise R. Beck, Hiroki Mashiko, Daniel M. Neumark & Stephen R. Leone (2013) Intensity dependence of light-induced states in transient absorption of laser-dressed helium measured with isolated attosecond pulses, Journal of Modern Optics, 60:17, 1506-1516, DOI: 10.1080/09500340.2013.826389

To link to this article: http://dx.doi.org/10.1080/09500340.2013.826389

PLEASE SCROLL DOWN FOR ARTICLE

Taylor & Francis makes every effort to ensure the accuracy of all the information (the "Content") contained in the publications on our platform. However, Taylor & Francis, our agents, and our licensors make no representations or warranties whatsoever as to the accuracy, completeness, or suitability for any purpose of the Content. Any opinions and views expressed in this publication are the opinions and views of the authors, and are not the views of or endorsed by Taylor & Francis. The accuracy of the Content should not be relied upon and should be independently verified with primary sources of information. Taylor and Francis shall not be liable for any losses, actions, claims, proceedings, demands, costs, expenses, damages, and other liabilities whatsoever or howsoever caused arising directly or indirectly in connection with, in relation to or arising out of the use of the Content.

This article may be used for research, teaching, and private study purposes. Any substantial or systematic reproduction, redistribution, reselling, loan, sub-licensing, systematic supply, or distribution in any form to anyone is expressly forbidden. Terms & Conditions of access and use can be found at http://www.tandfonline.com/page/terms-and-conditions

^a Department of Chemistry, University of California, and Chemical Sciences Division, Lawrence Berkeley National Laboratory, Berkeley, CA 94720, USA.

^b Department of Physics, University of California, Berkeley, CA 94720, USA. Published online: 02 Sep 2013.



Intensity dependence of light-induced states in transient absorption of laser-dressed helium measured with isolated attosecond pulses

M. Justine Bell^a, Annelise R. Beck^a, Hiroki Mashiko^{a†}, Daniel M. Neumark^{a*} and Stephen R. Leone^{a,b*}

^aDepartment of Chemistry, University of California, and Chemical Sciences Division, Lawrence Berkeley National Laboratory, Berkeley, CA 94720, USA; ^bDepartment of Physics, University of California, Berkeley, CA 94720, USA

(Received 30 April 2013; final version received 12 July 2013)

Light-induced states in He atoms were characterized using attosecond transient absorption spectroscopy. A 400 as pulse covering the $20-24 \,\mathrm{eV}$ spectral range serves as the probe pulse, and the effect of a few-cycle near infrared pulse (12 fs, 780 nm) on the absorption spectrum is measured as a function of time delay and near-infrared intensities varying from $(5.0\pm2)\times10^{10}$ to $(1\pm0.4)\times10^{13}\,\mathrm{W/cm^2}$. Light-induced states resulting from near-infrared coupling of 1s2p to 1s2s, 1s3d, and 1s3s states are observed. Absorption features that likely result from coupling of 1s3p to 1s4s, 1s4d, 1s5s, and 1s5d states are also observed. The light-induced states with the smallest detunings (1s3d and 1s3s) from the dressing frequency may shift to higher frequencies as the dressing intensity is increased.

Keywords: ultrafast optics; attosecond spectroscopy; dressed absorption; XUV

1. Introduction

Advances in laser and optical technology allow isolated attosecond pulses with durations less than 100 as and with spectral bandwidths as large as 75 eV to be produced [1]. Incorporating isolated attosecond pulses into time-resolved measurement schemes offers exciting opportunities for elucidation of chemical dynamics with time resolutions comparable to one atomic unit of time (~24 as) [2–7]. Recent work utilizes the broad bandwidth of isolated attosecond pulses for absorption spectroscopy measurements [8–12]. Attosecond time-resolved absorption spectroscopy experiments are especially applicable to monitoring dynamics occurring on a few fs time scale, including electronic wavepacket dynamics [8] and dynamics driven by a time dependent optical field [13,14].

Transient absorption spectroscopy, the technique of recording a transmitted spectrum of a laser pulse (probe pulse) as a function of delay time between the probe pulse and a second pulse (pump pulse), has been successful in measuring multi-femtosecond molecular dynamics for over two decades [15]. This technique is well suited to attosecond spectroscopy because isolated attosecond pulses necessarily have large bandwidths that allow spectral features over a broad range to be monitored. As examples, electronic coherence [8], modification of optical properties of insulating materials [16], and

lifetimes of autoionizing states [9] can be measured with attosecond transient absorption spectroscopy.

Owing to the limited number of photons in isolated attosecond pulses, typical attosecond pump-probe measurements incorporate a strong near infrared (NIR) pulse (intensities of 1012 W/cm2 or higher) together with the attosecond pulse. The NIR laser pulse can induce dynamics [8] or probe reaction products [17] (via field or multiphoton ionization), when overlapped in time with the XUV attosecond pulse. The strong NIR field can also couple atomic and molecular excited states resulting in a modified ('laser-dressed') absorption spectrum. Autler-Townes splittings, electromagnetically induced transparency [18,19], and light-induced states [20] have been measured for atoms in strong optical fields by femtosecond and attosecond XUV pulses. This paper focuses on light-induced states (LISs) [20], transient absorption features that occur when the attosecond and NIR pulses are overlapped in time and are not related to the field-free absorption spectra. These features are observed in the attosecond transient absorption spectra of laser-dressed helium and are experimentally manipulated as a function of NIR intensity on a few femtosecond timescale.

Most previous studies of laser dressed helium have utilized attosecond pulse trains. Laser dressed absorption has been used to control the ionization probability of helium by rescattering [21,22] and interference [23,24]

^{*}Corresponding authors. Email: srl@berkeley.edu; dneumark@berkeley.edu

[†]Present address: NTT Basic Research Lab, Quantum Optical Physics Research Group, Atsugi-shi, Kanagawa, 243-0198, Japan

studies of mechanisms. Theoretical laser-dressed absorption of attosecond pulse trains also identified a Raman-like multiphoton absorption process [25]. In the case of isolated attosecond pulses, recent work has focused on sub-optical cycle features [13,14], and the Raman-like two-photon mechanism occurring in the absorption spectra [20]. The second-order transitions observed in the dressed absorption spectra of helium in the range of the 1s2p transition are explored here with a broader range of NIR intensities $((5\pm2)\times10^{10}$ to $(1\pm0.4)\times10^{13}$ W/cm²) than utilized in Chen et al. [20]. The larger range of NIR intensities provides the opportunity to experimentally investigate the intensity dependence of the LISs. The NIR dressing intensity has two effects on the LISs: (1) additional LISs appear as the dressing intensity increases, and (2) the energies of the LISs may shift as the dressing intensity increases. The LISs result from the NIR laser coupling of the 1s2p state to the 1s3s, 1s3d, and 1s2s states of He. Both intensity dependent effects are related to the coupling strength and the detuning of the laser from the transition energy. The transient feature resulting from the $1s2p\rightarrow 1s2s$ (1s2s LIS) coupling is observed for intensities above $(1.5\pm0.6)\times10^{11}$, while the transient features resulting from $1s2p\rightarrow 1s3s$ (1s3s LIS) and $1s2p\rightarrow 1s3d$ (1s3d LIS) are seen at intensities above $(7.5\pm3)\times10^{10}$. Above intensities of $(5\pm2)\times10^{12}\,\mathrm{W/cm^2}$ absorption features that possibly correspond to 1s4s, 1s4d, 1s5s and 1s5d LISs are observed. For intensities between $(7.5\pm3)\times$ 10^{10} and $(1.5 \pm 0.6) \times 10^{12} \,\mathrm{W/cm^2}$, the 1s3s and 1s3d LIS may increase in energy as the NIR intensity is increased. The other absorption features are relatively stable.

2. Experimental methods

2.1. Attosecond pulse generation and transient absorption spectrometer

The spectrometer has been described previously [20] and is diagrammed in Figure 1. Briefly, isolated attosecond pulses are generated via high harmonic generation (HHG) with double optical gating (DOG) [26,27] in a cell filled with 2.7 hPa (2 Torr) krypton gas. The DOG optics are selected so that the HHG gate width is 1.8 fs, which means that in the present case only one isolated attosecond pulse will be generated when driving harmonic generation even though the driving pulse is not carrier-envelope phase-stabilized [28]. An f = 25 cm Ru/Si multilayer mirror focuses the attosecond and NIR pulses into a 1 mm long absorption cell and an f = 25 cm Mo/Si multilayer mirror directs the transmitted attosecond pulse onto an aberration corrected gold coated grating (1200 grooves/mm). An X-ray chargecoupled device (CCD) camera records the dispersed spectrum. The resulting spectral resolution is 100 meV. An interferometer incorporating an actively stabilized piezo transducer delay stage controls the delay between the NIR and attosecond pulses. In the interferometer, an annular hole mirror separates the incoming beam into an inner circular portion to drive HHG and an outer ring that serves as the optical dressing field. A neutral density filter controls the intensity of the NIR field.

Spectral interferometry for direct reconstruction of the electric field (SPIDER) [29] measurements characterize the 12 fs long NIR pulse. The NIR pulses are longer than the 7 fs pulses that drive HHG because the spectral broadening from the hollow-core fiber used for few-cycle pulse generation is weaker near the edges of the beam. Photoelectron streaking [30] measurements and the frequency-resolved optical gating for complete reconstruction of attosecond bursts (FROG-CRAB) technique with the principal components generalized projection algorithm (PCGPA) [31–33] characterize the attosecond pulse.

DOG produces attosecond pulses with a measured duration of 145 ± 10 as when a 200 nm thick Al filter (band-pass of 18-72 eV) is used to remove the residual NIR field. A 200 nm thick Sn filter (band-pass of 15-24 eV) limits the XUV spectrum to energies just below the ionization potential of He and prevents second order diffraction of ~40-50 eV photons from overlapping with first order diffraction of $\sim 20-25 \,\mathrm{eV}$ photons on the CCD camera. The resulting attosecond pulse covers the spectral range of 20-24 eV and its duration is 380 ± 10 as, limited by the 24 eV high energy cutoff of the Sn filter. Material dispersion from Sn filters used to select the bandwidth of the attosecond pulse in conjunction with phase effects from the HHG process and the XUV multilayer mirror also contribute to the pulse duration.

The absorption target cell is a $\sim 1 \text{ mm}$ diameter cylindrical tube. The attosecond and NIR beams pass though apertures laser-drilled by the femtosecond NIR HHG driver pulse prior to experiments. Gaussian beam propagation equations estimate the NIR beam diameter (twice the beam waist) at the cell walls to be $\sim 300 \, \text{um}$. placing an upper limit on the aperture diameter. Calibration of target gas densities uses the absorption continuum above the He ionization potential at 24.58 eV; this procedure is similar to the methods used by Loh et al. [34] to estimate target density of xenon in transient absorption measurements. Estimating the target pressure using absorption above the ionization continuum limits any effect that the relatively broad spectral resolution may have on estimating target density from much narrower absorption lines (for example, at room temperature the Doppler broadened bandwidth of the 1s2p resonance is on the order of 0.1 meV, while the experimental resolution is 100 meV). This calibration is performed using Xe as the HHG medium, since it has a harmonic cut-off low enough to prevent second order diffraction from

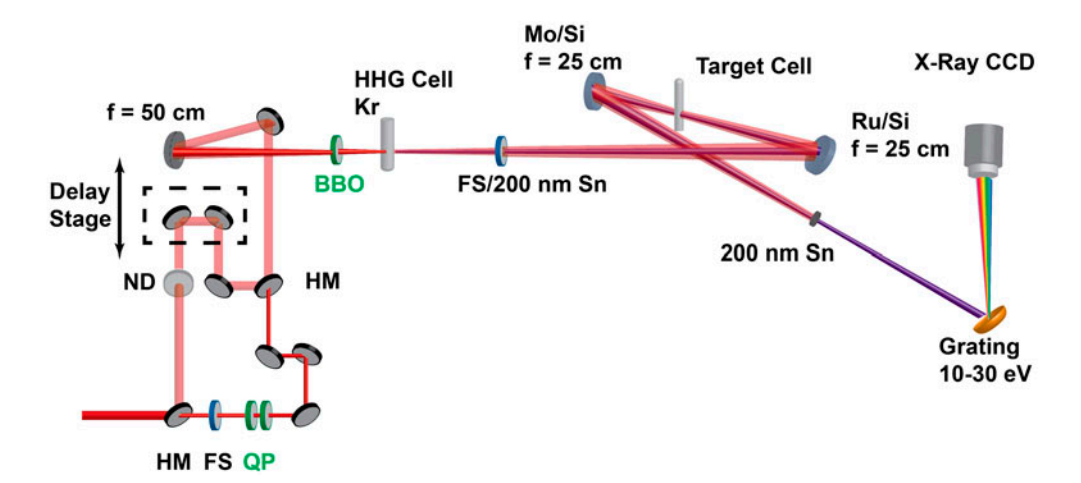


Figure 1. Attosecond transient absorption apparatus. HM: hole mirrors; ND: neutral density filter; QP: quartz plates; BBO: β -BaB $_2$ O $_4$. The delay stage has a ± 50 as rms jitter over 24 hours. The DOG optics are shown in green. (The color version of this figure is included in the online version of the journal.)

overlapping first order diffraction on the CCD camera. An Al filter that, unlike the Sn filter, transmits photon energies above the ionization potential of the He is used to block the residual NIR light. The NIR laser intensity is estimated using the in situ streaking shift measured in photoelectron streaking measurements. The $1/e^2$ width of the NIR beam is $90\pm10\,\mu\text{m}$, measured by removing the absorption cell and inserting a CCD camera into the focus in the interaction region. Gaussian beam propagation estimates that the $1/e^2$ width of the XUV beam at the focus is $15\pm1\,\mu\text{m}$.

The absorption spectra in Section 3 use the transmitted spectra of the attosecond pulse (without any He gas in the absorption cell) as a reference. Negative pumpprobe delays correspond to cases where the attosecond pulse arrives at the target cell before the NIR pulse.

3. Experimental results

3.1. Static absorption spectra

The energy levels of atomic He accessible by one photon of the attosecond pulse are plotted in Figure 2(a). The transmitted spectra of the attosecond pulse with and without the He target gas are plotted in Figure 2(b) and the absolute optical density, $OD(\omega)$, is plotted in Figure 2(c). The absolute optical density is given by:

$$OD(\omega) = -\log[I_f(\omega)/I_i(\omega)], \tag{1}$$

where $I_i(\omega)$ is the initial spectra recorded without He target gas, and $I_f(\omega)$ is the transmitted spectrum with He target gas present. The target gas density is 1.6 \pm 0.05 hPa. Peaks in the absorption spectrum corresponding to the 1s2p, 1s3p, and 1s4p transitions at 21.21, 23.09, and 23.74 eV [35] shown in Figure 2(a) are visible in the *OD* plotted in Figure 2(c).

3.2. Transient absorption spectra

The transient absorption spectra are given by:

$$OD(\omega, t) = -\log[I_t(\omega)/I_i(\omega)],$$
 (2)

where $I_t(\omega)$ is the transmitted spectrum of the attosecond pulse recorded with He target gas and at pump–probe delay t. Figures 3 and 4 show transient absorption spectra plotted against pump–probe delay time for NIR intensities ranging from $(5.0\pm2)\times10^{10}$ W/cm² to $(1\pm0.4)\times10^{13}$ W/cm². This range of intensities, over two orders of magnitude, is more extensive than previously studied [20] and allows the intensity dependence of transient features to be investigated. Spectra were recorded for 1.5×10^5 laser pulses at each time delay step, with He target gas at a pressure of 1.6 ± 0.05 hPa.

The transient absorption spectrum recorded with the lowest NIR laser intensity, $I_0 = (5.0 \pm 2) \times 10^{10} \,\mathrm{W/cm^2}$, is plotted in Figure 3(a). For positive pump–probe delays, the NIR pulse arrives at the target before the attosecond pulse and only features that directly correspond to the field-free absorption spectra in Figure 2 are visible. At zero pump–probe delay, the attosecond pulse and the NIR pulse are overlapped in time in the gas target, and a weak transient absorption feature is visible around 21.5 eV.

As the NIR intensity is increased, the transient features become more pronounced. Figures 3(b)-(c) show transient absorption spectra recorded at NIR intensities of $1.5I_0$ and $3I_0$, respectively. In Figures 3(b)-(c), two transient features A and B that are not due to the field-free absorption spectra of He are visible near 21.25 eV and 21.5 eV, respectively. Feature B is well separated from the 1s2p absorption peak at 21.2 eV, while feature A begins to emerge as a shoulder on the 1s2p absorption peak. The centroid of each feature, as a function of

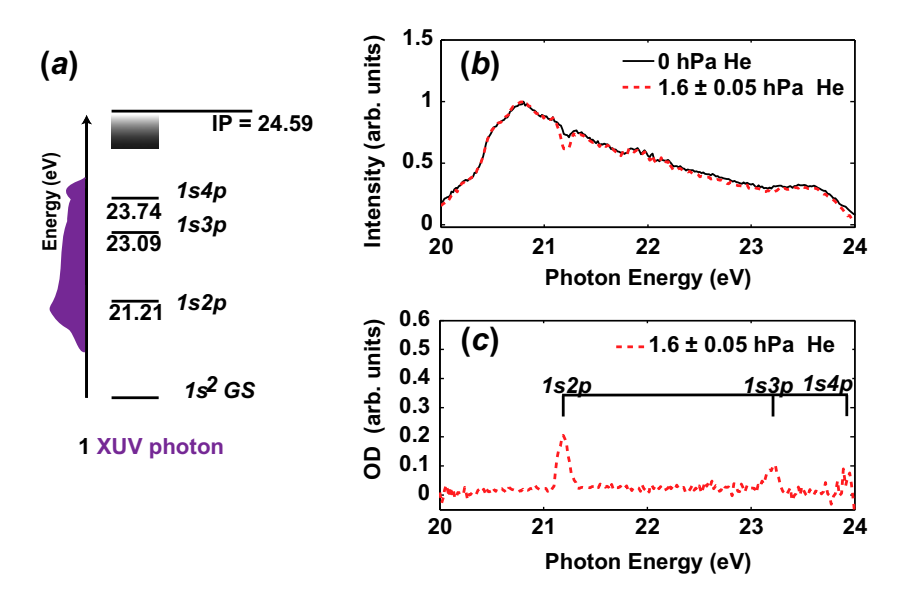


Figure 2. States of helium accessible in experiments. (a) Atomic states of helium in the range of the attosecond pulse. (b) Transmitted spectrum of helium and (c) OD calculated from the spectrum in (b). Transitions from $1s^2$ ground state to 1s2p, 1s3p, and 1s4p states are labeled in (c). (The color version of this figure is included in the online version of the journal.)

pump-probe delay, has been superimposed on top of the two dimensional pump-probe experimental spectra in magenta to guide the eye. The absorption features shift in energy across the pump-probe delay scan, so defining a feature by a particular energy is difficult, but the centroids clearly identify the spectral features.

As in Figure 3(a), only absorption corresponding to field-free absorption are visible at large positive pump-probe delays. For negative pump-probe delays (the attosecond XUV pulse arrives at the target before the NIR pulse), the spectra appear to be broadened and increase in intensity. There is also an asymmetry; the absorption features at negative pumpprobe delays appear stronger. As in Chen et al. [20], the asymmetry is attributed to the increased broadening of the helium absorption lines by the NIR laser, appearing as increased absorption due to detector saturation at the transition frequencies. Figures 4(a)-(c) show the transient absorption spectra recorded with NIR intensities of $30I_0$, $100I_0$, and $200I_0$. In Figure 4(a), features A and B are visible, and a new feature, C, near 22 eV appears. The 1s2p absorption line has split into a lower energy component at 21.00 eV and feature A. In Figures 4(b)-(c), two new features, E and F, near 22.2 and 22.4 eV, respectively, are visible near zero delay. Similar to the spectra plotted in Figure 3, the absorption spectra plotted in Figure 4 are asymmetric with respect to pump-probe delay; the absorption features are stronger for negative pump-probe delays.

Line spectra at zero fs delay are plotted in Figure 5. In the line spectra measured with $1.5I_0$, $3I_0$, and $30I_0$ (plotted in Figure 5 in teal, magenta, and green), the peaks A, B and the 1s2p peak shift in energy. Comparing

the spectra measured with $1.5I_0$ to $3I_0$, the 1s2p absorption feature broadens and shifts lower in energy and shoulder A begins to separate from the 1s2p absorption peak as the intensity is increased. As the intensity increases from $3I_0$ to $30I_0$, feature A and the lower energy component of 1s2p further split. Feature B slightly increases in energy as the intensity is increased from $1.5I_0$ to $3I_0$ and again as the intensity is increased from $3I_0$ to $30I_0$. At intensities of $100I_0$ and $200I_0$, no clear shifts in peak position are observed. The peak positions at zero fs delay are listed in Table 1.

The origin of the new transient absorption features and the splitting of the 1s2p absorption feature at the overlap of the XUV attosecond pulse and the NIR pulse will be discussed in more detail in Section 4. Possible changes in the photon energies of the absorption features and the variations with intensity necessary to observe the features will be discussed.

4. Analysis and discussion

Near zero pump-probe delay, features in the absorption spectra that are not present in the field-free absorption spectra occur (for example, at 21.25 eV and 21.50 eV in Figure 5). Following the approach in Chen at al. [20], the absorption features near zero femtoseconds pump-probe delay are interpreted as light induced states (LISs) that are the intermediate step in Raman-like two-photon transitions from the ground state of He to 1sns and 1snd excited states of He. Similar multiphoton mechanisms are identified for dressed absorption of attosecond pulse trains [25]. The two-photon pathway is shown:

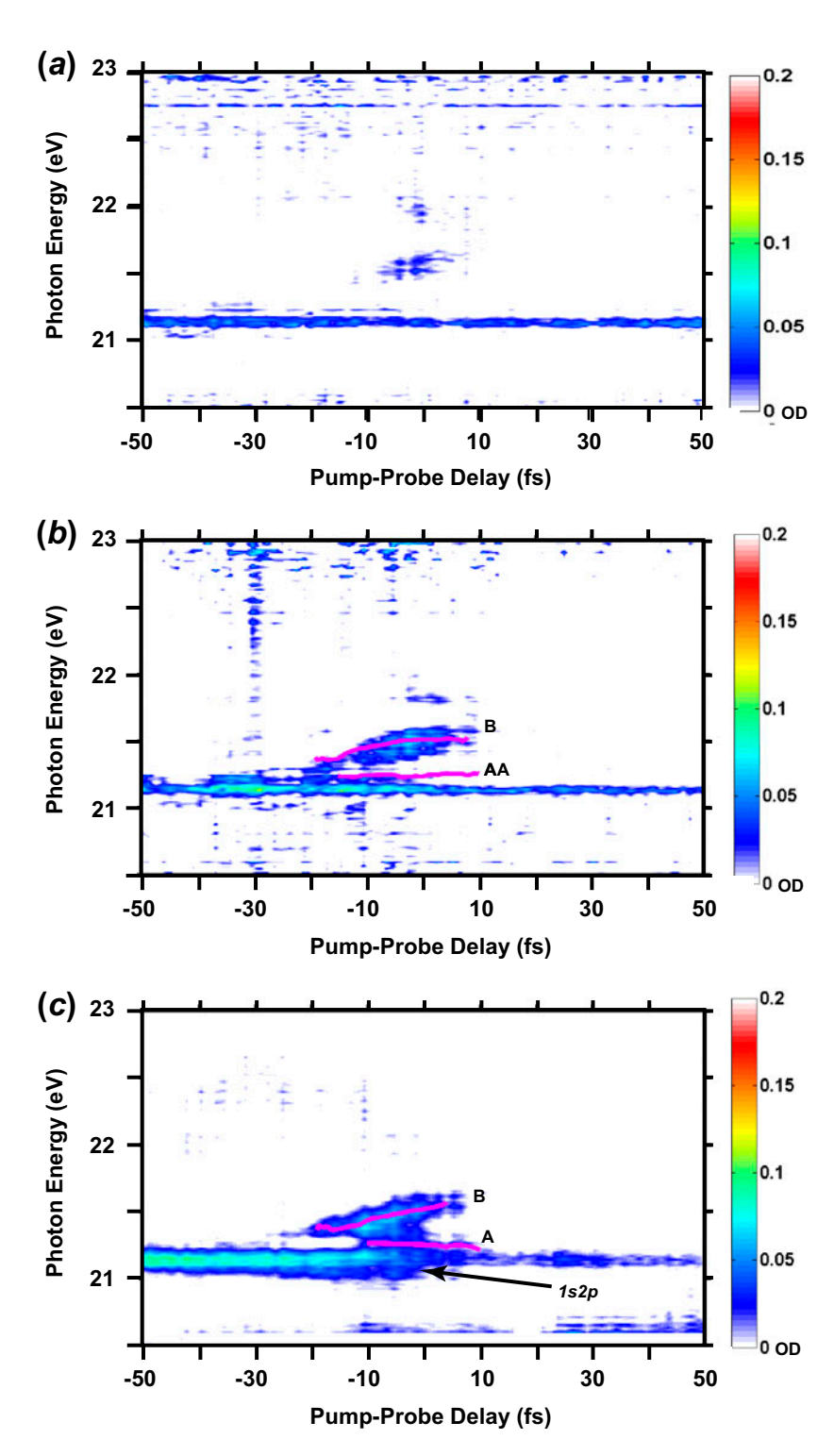


Figure 3. Transient absorption spectra recorded with NIR intensity of $I_0 = 5$. $0 \pm 2 \times 10^{10} \,\text{W/cm}^2$ (a), $1.5I_0$ (b), and $3I_0$ (c). Features near zero femtosecond delay are labeled according to the text and the centroid of each peak, as function of pump–probe delay, is superimposed in magenta. (The color version of this figure is included in the online version of the journal.)

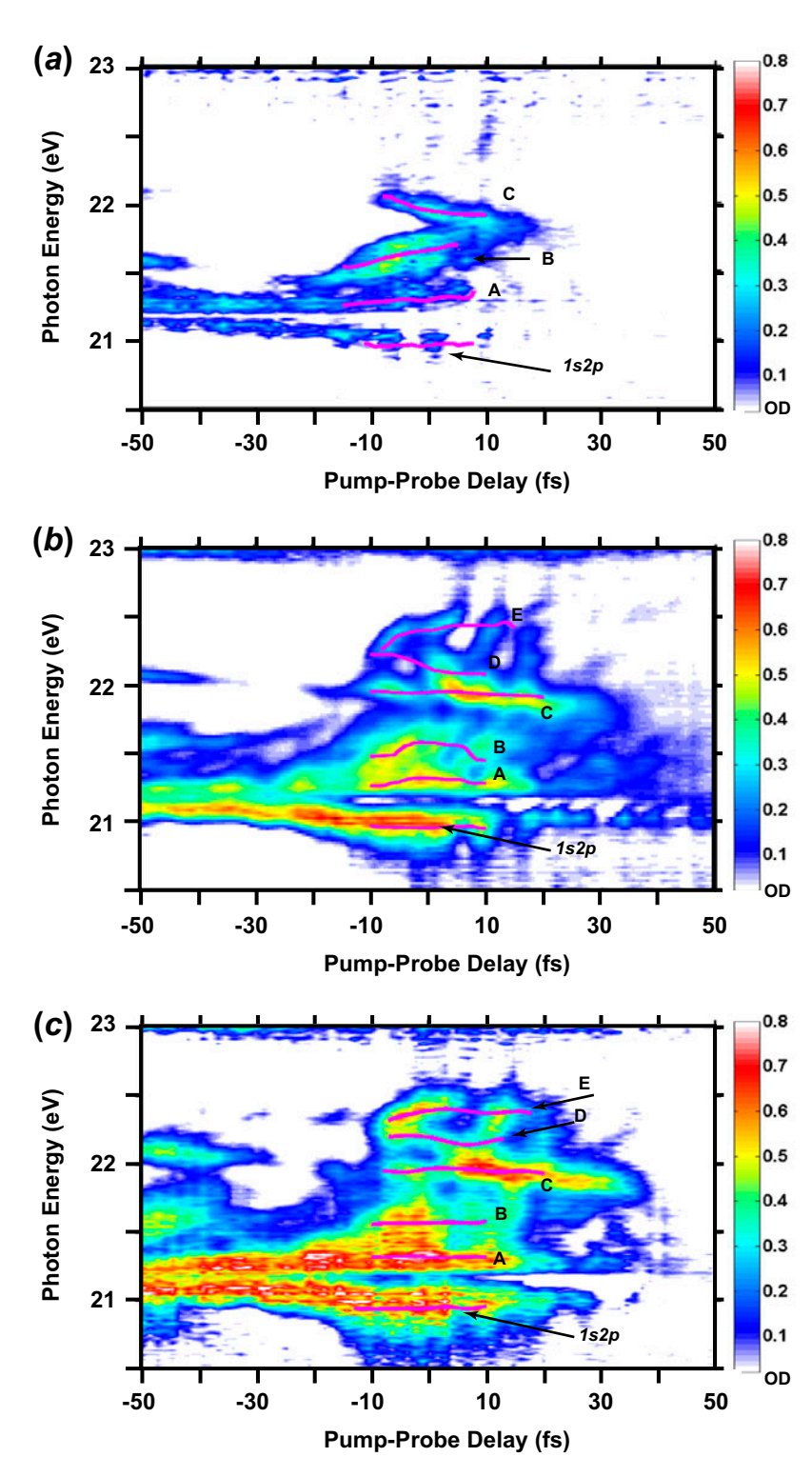


Figure 4. Transient absorption spectra recorded with NIR intensity of $30I_0$ (a), $100I_0$ (b), and $200I_0$ (c). Features near zero delay are labeled according to the text and the centroid of each peak is superimposed in magenta. (The color version of this figure is included in the online version of the journal.)

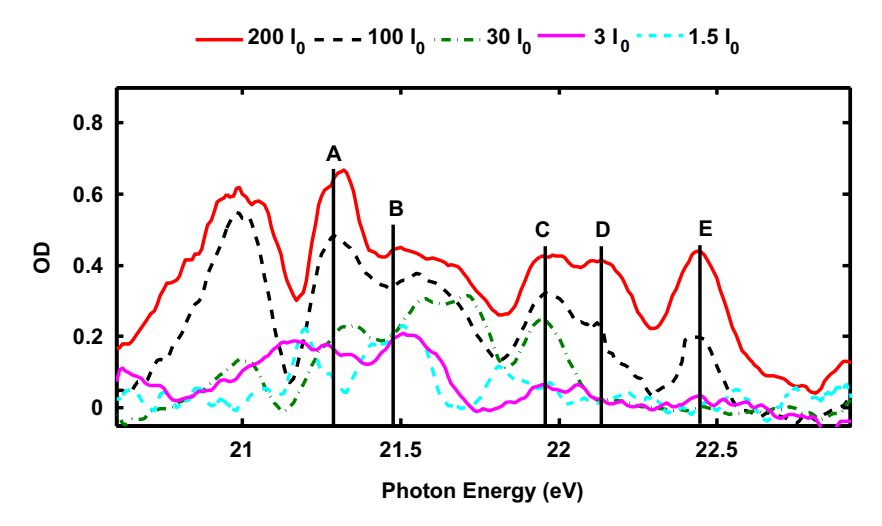


Figure 5. Line spectra at zero femtosecond pump–probe delay recorded with NIR intensity of 200 (red solid), 100 (black dashed), 30 (green dot-dashed), 3 (magenta solid) and 1.5 (teal dashed) I_0 . Results for 3 and 1.5 I_0 have been scaled by a factor of 3. Features near zero femtosecond delay are labeled according to the text. Vertical lines correspond to two-photon transitions described in Section 4. (The color version of this figure is included in the online version of the journal.)

Table 1. Peaks identified at the overlap of NIR and XUV attosecond pulse.

Intensity	1s2p	Peak position (eV)						
		A	В	С	D	Е		
$1.5I_0$	21.20	21.25	21.50					
$3I_0$	21.15	21.30	21.55					
$30I_{0}$	21.00	21.35	21.65	21.95				
$100I_{0}$	20.95	~21.3	~21.6	21.95	22.15	22.4		
$200I_0$	20.95	~21.3	~21.6	21.95	22.15	22.4		

Positions of absorption features at zero pump-probe delay. The positions are taken as the value of the centroids plotted in Figures 3 and 4 at 0 fs.

$$1s^{2} \xrightarrow{hv_{XUV}} 1s3s \quad LIS \text{ (feature A)} \xrightarrow{+hv_{NIR}} 1s3s$$

$$1s^{2} \xrightarrow{hv_{XUV}} 1s3d \quad LIS \text{ (feature B)} \xrightarrow{+hv_{NIR}} 1s3d$$

$$1s^{2} \xrightarrow{hv_{XUV}} 1s2s \quad LIS \text{ (feature C)} \xrightarrow{-hv_{NIR}} 1s2s \tag{3}$$

$$1s^{2} \xrightarrow{hv_{XUV}} 1s4s/d \quad LIS \text{ (feature D)} \xrightarrow{+hv_{NIR}} 1s4s/d$$

$$1s^{2} \xrightarrow{hv_{XUV}} 1s5s/d \quad LIS \text{ (feature E)} \xrightarrow{+hv_{NIR}} 1s5s/d.$$

The energies of the LIS are approximately:

$$\hbar\omega_{A} = \hbar\omega_{1s3s \ LIS} \approx \hbar\omega_{1s3s} - \hbar\omega_{NIR}
\hbar\omega_{B} = \hbar\omega_{1s3d \ LIS} \approx \hbar\omega_{1s3d} - \hbar\omega_{NIR}
\hbar\omega_{C} = \hbar\omega_{1s2s \ LIS} \approx \hbar\omega_{1s2s} + \hbar\omega_{NIR}
\hbar\omega_{D} = \hbar\omega_{1s4s/d \ LIS} \approx \hbar\omega_{1s4s/d} - \hbar\omega_{NIR}
\hbar\omega_{E} = \hbar\omega_{1s5s/d \ LIS} \approx \hbar\omega_{1s5s/d} - \hbar\omega_{NIR}$$
(4)

Vertical lines plotted in Figure 5 correspond to the energies given by Equation (4). The energy of the 1s2s LIS (feature C at 21.95 eV) is offset from the value given by Equation (4) (22.21 eV). The two-photon transitions are diagrammed in Figure 6. For example, the

absorption features A and B at 21.25 and $21.50 \,\mathrm{eV}$ in Figure 4(a) result from absorption of one photon from the XUV attosecond pulse and absorption of one photon of NIR to reach, respectively, the 1s3s and 1s3d states of He. Similarly, feature C at $21.95 \,\mathrm{eV}$ in Figure 4(a) acts as the intermediate step in a two-photon pathway connecting the ground state to the 1s2s state by absorption of one XUV photon and emission of one NIR photon. Features D and E in Figures 4(b)-(c), which were not previously observed in lower intensity measurements, may be the intermediate step in two-photon absorption process to reach the 1s4s and 1s4d (D) states and the 1s5s and 1s5d (E) states of He, analogous to the mechanism producing features A and B.

The experimental resolution (0.1 eV) combined with the NIR laser bandwidth (0.3 eV) prevents the 1s4s and 1s4d or the 1s5s and 1s5d LIS from being resolved. At intensities of $100I_0$ and $200I_0$, the absorption spectra become increasingly complex near zero delay with broad absorption features possibly due to multiplet splitting of the LISs. Multiplet splitting of absorption features is predicted [11] and observed [19] for high-field dressed

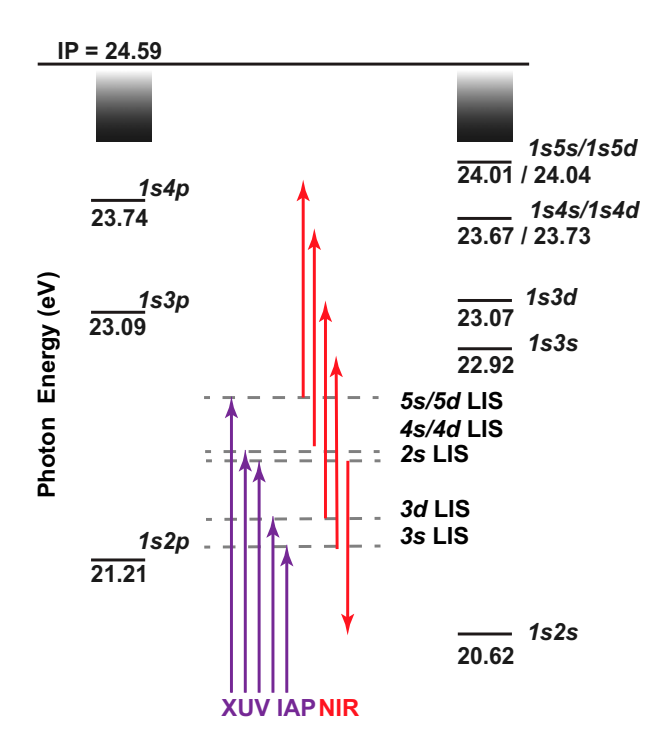


Figure 6. Mechanism for light induced states. The attosecond XUV pulse where the NIR field (red arrows) couple the states to surrounding *n*s and *n*d states. (The color version of this figure is included in the online version of the journal.)

absorption measurements of atomic xenon in the XUV spectral region. Due to the possibility of multiplet splitting and increasing complexity of the absorption spectra, the assignment of the 1s4s/d and 1s5s/d LISs is tentative. Equations (3)–(4) are convenient for identifying the new absorption features, but the equations do not directly identify which states of helium are interacting.

Figure 7 compares the calculated positions of the 1s2s, 1s3d, and 1s3s LISs from Chen et al. [20] with the

experimentally observed features C, B, and A as a function of field intensity. In the calculations, the single atom frequency dependent responses have been calculated using the methods detailed in [36]. For intensities up to $30I_0$, the positions of features A and B are reasonably correlated to the calculated positions of the 1s3s and 1s3d LISs. At higher intensities there is a discrepancy between features A and B and the calculated positions of the LISs. The inconsistency between the calculations and the current experimental results (in addition to similar behavior observed in [14]) suggests future experimental studies. The exact cause of the discrepancy between the experimental and theoretical results in Figure 7 is unknown at this time. Due to experimental stability considerations, the NIR laser intensity is scanned in relatively large steps. The coarse steps may lose some of the subtlety of the theoretical calculations and account for some differences between the current results and [20]. Shifts in LIS positions may be more apparent with a finer intensity scan. Differences in the experimental and theoretical spectra are also expected due to intensity averaging over the interaction volume, pulse to pulse fluctuations in intensity and spectral phase, and macroscopic absorption effects in the experimental interaction volume. Future experiments with smaller interaction volumes and lower target densities may help mitigate some of these effects. With this in mind, the analysis will focus on why the energies of the 1s3s and 1s3d LIS may be sensitive to changes in the field intensity (at least for intensities between $1.5I_0$ and $30I_0$).

Further analysis of the positions of the LISs utilizes the dressed absorption perspective, where a manifold of states that correspond to the emission and absorption of successive NIR laser photons are coupled [37,38]. When the energy difference between the field-free transition frequency and the dressing frequency $(\hbar\omega_{1s2p} - \hbar\omega_{NIR})$

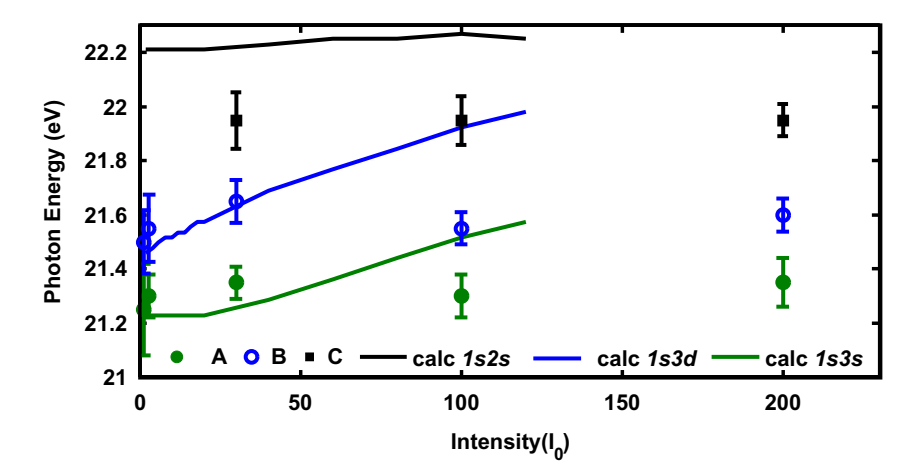


Figure 7. The positions of the experimental absorption features A (green filled circles), B (blue open circles), and C (black filled squares) are plotted as a function of dressing intensity. The calculated positions of the LISs from [20] are plotted for comparison. (The color version of this figure is included in the online version of the journal.)

is large compared to the interaction between the coupled states, dressed absorption can be interpreted as twophoton transitions, similar to the Raman-like mechanism described previously [37]. This interpretation explicitly takes into account which field-free states are interacting without calculating the polarization field (as in prior XUV dressed absorption calculations [10,11,20,36]). The following model is less sophisticated than methods of Chen at al. [20] and Gaarde et al. [36], where the timedependent Schrödinger equation for a quantum atom in a semi-classical electric field is solved. The non-perturbative calculations by Chen, Gaarde, and co-workers include effects that depend on the electric field at many degrees of nonlinearity. However, the model described here can provide insight into dressed absorption with a significantly smaller layout of computational resources.

The second-order perturbation theory correction to the energy of a state (E_n) in an oscillating electric field is given by [37,38]:

$$E_{n} = \frac{1}{4} \sum_{m \neq n} \left\{ \frac{|\overrightarrow{E_{\theta}} \bullet \overrightarrow{d_{nm}}|^{2}}{E_{n} - E_{m} - \hbar \omega_{NIR}} + \frac{|\overrightarrow{E_{\theta}} \bullet \overrightarrow{d_{nm}}|^{2}}{E_{n} - E_{m} + \hbar \omega_{NIR}} \right\} (5)$$

where $\overrightarrow{E_{\theta}}$ is the electric field vector, $\overrightarrow{d_{nm}}$ is the transition dipole between field-free states n and m with energies E_n and E_m , respectively. In the present case, the 1s2p state is coupled to the 1s3s, 1s3d, and 1s2s states via one-photon transitions, resulting in features A, B, and C and a shifted 1s2p absorption peak. Features D and E in Figures 4(b)-(c) may result from either the 1s2p or the 1s3p coupling to the 1s4s/d and 1s5s/d states via one-photon transitions. The 1s3p state is expected to have the larger contribution because the NIR photon energy is close to resonance for the 1s3p \rightarrow 1s4s/d and 1s3p \rightarrow 1s5s/d transitions than for the 1s2p \rightarrow 1s4s/d and 1s2p \rightarrow 1s5s/d transitions and the transition dipoles for the 1s3p \rightarrow 1s4s/d and 1s3p \rightarrow 1s5s/d pathways are larger [39].

Equation (5) depends on the magnitude of $\overrightarrow{d_{nm}} \bullet \overrightarrow{E_{\theta}}$ and the energy difference between the atomic transition

the photon energy of the dressing (i.e. the detuning). The detunings of the dressing laser frequency from the field-free atomic transition and the Rabi frequencies $(\Omega_R = \frac{-1}{\hbar} \overrightarrow{d_{nm}} \bullet \overrightarrow{E_{\theta}})$ calculated at $30I_0$ (1.5 × 10^{12} W/cm²) are listed in Table 2. These values correspond to the denominator and numerator terms in Equation (5). Also listed in Table 2 are the E_n for the LIS calculated from Equation (5). For example, the detuning for the 1s3s LIS, (feature A), is smaller than the Rabi frequency, therefore the E_n calculated from Equation (5) is larger than the converse case. The central energy of the NIR laser is $\sim 1.6 \, \text{eV}$ ($\sim 90 \, \text{THz}$), and the bandwidth is $\sim 0.3 \text{ eV}$ ($\sim 73 \text{ THz}$), so the 1s3s and 1s3d LISs are resonant or near-resonant with the laser frequency. Transition dipoles are taken from [39]. The field intensity used to calculate the parameters in Table 2 is $30I_0$, because $30I_0$ is the largest intensity where a shift in energy is observed in experimental results. The shifts in Figure 7 calculated by Chen et al. [20], however, increase at higher intensities.

From Table 2, the detunings for the 1s3s and 1s3d LIS (features A and B) are considerably smaller than the detunings for the other LISs (features C, D, and E), therefore the 1s3s and 1s3d LIS are expected to appear at lower NIR field strengths. Direct comparison of the onset intensities between the n=4 and 5 LIS and the n=2 and 3 LIS may be complicated because the n=4 and 5 LISs most likely result from coupling of the 1s3p state while the n=2 and 3 LISs result from coupling of the 1s2p state.

Equation (5) yields the largest energy corrections for the 1s3s and 1s3d LIS (features A and B). These are the states that are closest to resonance with the NIR coupling field, and the states that may increase in energy as the field intensity increases at field intensities up to $30I_0$. Equation (5) overestimates the energy shifts, as compared to the results of Chen et al. [20] in Figure 7, but both Chen et al. and Equation (5) predict the smallest shift for the 1s2s LIS. Equation (5) serves as a cursory gauge of relative tendency of LIS to shift in response to

Table 2. The detunings, Rabi frequencies, and E_n of the LISs.

LIS	Feature			Rabi frequency			
		Detuning		at $30I_0$ $1.5 \times 10^{12} \text{ (W/cm}^2\text{)}$		E_n	
		(THz)	(eV)	(THz)	(eV)	(THz)	(eV)
1s3s	A	-26	-0.11	80	0.3	60	0.26
1s3d	B	-62	-0.26	130	0.55	75	0.31
1s2s	C	240	1	220	0.9	25	0.11
1s4s/1s4d	D	-240	-1	210	0.85	-25	-0.1
1s5s/1s5d	E	-170	-0.7	80	0.3	-7	-0.03

The transition dipoles are taken from [38]. The detunings, Rabi frequencies, and E_n calculated from Equation (5). Both frequency and energy units are given. The LISs that have the largest E_n have the largest ratio of Rabi frequency to detuning.

field intensity. The coupling also results in the 1s2p absorption peak decreasing in energy as the field intensity increases; however, due to the multiple couplings of the 1s2p state (for example coupling to the 1s2s, 1s3s, and 1s3d states) the intensity dependence of the 1s2p state is not straightforward to interpret.

5. Conclusions

Attosecond transient absorption spectroscopy employed to measure the intensity dependence of LISs in the absorption spectra of helium in the region of the 1s2p resonance at 21.21 eV. At intensities of (7.5 ± 3) × 10¹⁰ W/cm² LISs resulting from coupling of 1s2p to 1s3d and 1s3s states are observed, while the LIS resulting from the coupling of 1s2p to 1s2s state is visible at intensities of $(1.5 \pm 0.6) \times 10^{11}$ W/cm². Above intensities of $(5\pm2)\times10^{12}$ W/cm² new absorption features that likely correspond to 1s4s/d and 1s5s/d LISs are observed. At intensities of $(1.5 \pm 0.6) \times 10^{11}$ W/cm², the 1s3s and 1s3d LISs may increase in energy as the NIR intensity is increases. The possible shift in energy with NIR intensity is attributed to a small detuning, -62 THz or -26 THz (-0.26 or -0.11 eV), for the $1s2p \rightarrow 1s3d$ and 1s2p→1s3s transitions. These considerations will be useful for the preparation state specific samples in future measurements, as well as future attosecond pump-probe spectroscopy measurements, where the wavelength and intensities of the optical pulses can be selected so that specific atomic and molecular states are affected more strongly than others. For example in attosecond transient absorption measurements of autoionization lifetimes, the optical pulse can be selected to strongly couple an autoionization resonance to other nearby states, or the optical pulse can be selected to favor a multiphoton ionization process.

Acknowledgements

This work was supported by the Director, Office of Science, Office of Basic Energy Sciences, and by the Division of Chemical Sciences, Geosciences, and Biosciences of the U.S. Department of Energy at LBNL under Contract No. DE-AC02-05CH11231. M.J.B. and A.R.B. acknowledge funding from NSF-GRFP. S.R.L acknowledges the support of a National Security Science and Engineering Faculty Fellowship. T. Pfeiffer, A.N. Pfeiffer are thanked for helpful discussions of experimental details.

References

- [1] Zhao, K.; Zhang, Q.; Chini, M.; Wu, Y.; Wang, X.; Chang, Z. Opt. Lett. 2012, 37, 3891–3893.
- [2] Drescher, M.; Hentschel, M.; Kienberger, R.; Uiberacker, M.; Yakovlev, V.; Scrinzi, A.; Westerwalbesloh, T.; Kleineberg, U.; Heinzmann, U.; Krausz, F. *Nature (London, U. K.)* 2002, 419, 803–807.
- [3] Pfeifer, T.; Abel, M.J.; Nagel, P.M.; Jullien, A.; Loh, Z.-H.; Bell, M.J.; Neumark, D.M.; Leone, S.R. Chem. Phys. Lett. 2008, 463, 11–24.

- [4] Krausz, F.; Ivanov, M. Rev. Mod. Phys. 2009, 81, 163-234.
- [5] Yakovlev, V.S.; Gagnon, J.; Karpowicz, N.; Krausz, F. Phys. Rev. Lett. 2010, 105, 073001.
- [6] Gallmann, L.; Cirelli, C.; Keller, U. Annu. Rev. Phys. Chem. 2012, 63, 447–469.
- [7] Prell, J.S.; Borja, L.J.; Neumark, D.M.; Leone, S.R. Ann. Phys. (Berlin) 2013, 525, 151–161.
- [8] Goulielmakis, E.; Loh, Z.-H.; Wirth, A.; Santra, R.; Rohringer, N.; Yakovlev, V.S.; Zherebtsov, S.; Pfeifer, T.; Azzeer, A.M.; Kling, M.F.; Leone, S.R.; Krausz, F. *Nature* (London, U.K.) 2010, 466, 739–744.
- [9] Wang, H.; Chini, M.; Chen, S.; Zhang, C.-H.; He, F.; Cheng, Y.; Wu, Y.; Thumm, U.; Chang, Z. Phys. Rev. Lett. 2010, 105, 143002.
- [10] Santra, R.; Yakovlev, V.S.; Pfeifer, T.; Loh, Z.-H. Phys. Rev. A: At., Mol., Opt. Phys. 2011, 83, 033405.
- [11] Pfeiffer, A.N.; Leone, S.R. Phys. Rev. A: At., Mol., Opt. Phys. 2012, 85, 053422.
- [12] Loh, Z.-H.; Leone, S.R. J. Phys. Chem. Lett. 2013, 4, 292–302.
- [13] Chini, M.; Zhao, B.; Wang, H.; Cheng, Y.; Hu, S.; Chang, Z. Phys. Rev. Lett. 2012, 109, 073601.
- [14] Chini, M.; Wang, X.; Cheng, Y.; Wu, Y.; Zhao, D.; Telnov, D.A.; Chu, S.-I.; Chang, Z. Sci. Rep. 2013, 3, 1105.
- [15] Pollard, W.T.; Mathies, R.A. Annu. Rev. Phys. Chem. 1992, 43, 497–523.
- [16] Schultze, M.; Bothschafter, E.M.; Sommer, A.; Holzner, S.; Schweinberger, W.; Fiess, M.; Hofstetter, M.; Kienberger, R.; Apalkov, V.; Yakovlev, V.S.; Stockman, M.I.; Krausz, F. *Nature (London, U.K.)* 2012, 493, 75–78.
- [17] Uiberacker, M.; Uphues, T.; Schultze, M.; Verhoef, A.J.; Yakovlev, V.; Kling, M.F.; Rauschenberger, J.; Kabachnik, N.M.; Schröder, H.; Lezius, M.; Kompa, K.L.; Muller, H.-G.; Vrakking, M.J.J.; Hendel, S.; Kleineberg, U.; Heinzmann, U.; Drescher, M.; Krausz, F. Nature (London, U.K.) 2007, 446, 627–632.
- [18] Loh, Z.-H.; Greene, C.H.; Leone, S.R. Chem. Phys. 2008, 350, 7–13.
- [19] Lin, M.-F.; Pfeiffer, A.N.; Neumark, D.M.; Leone, S.R.; Gessner, O. J. Chem. Phys. 2012, 137, 244305.
- [20] Chen, S.; Bell, M.J.; Beck, A.R.; Mashiko, H.; Wu, M.; Pfeiffer, A.N.; Gaarde, M.B.; Neumark, D.M.; Leone, S. R.; Schafer, K.J. *Phys. Rev. A: At., Mol., Opt. Phys.* **2012**, 86, 063408.
- [21] Holler, M.; Schapper, F.; Gallmann, L.; Keller, U. Phys. Rev. Lett. 2011, 106, 123601.
- [22] Johnsson, P.; Mauritsson, J.; Remetter, T.; L'Huillier, A.; Schafer, K.J. Phys. Rev. Lett. 2007, 99, 233001.
- [23] Shivaram, N.; Timmers, H.; Tong, X.-M.; Sandhu, A. Phys. Rev. A: At., Mol., Opt. Phys. 2012, 85, 05180R.
- [24] Ranitovic, P.; Tong, X.M.; Hogle, C.W.; Zhou, X.; Liu, Y.; Toshima, N.; Murnane, M.M.; Kapteyn, H.C. *Phys. Rev. Lett.* **2011**, *106*, 193008.
- [25] Chen, S.; Schafer, K.J.; Gaarde, M.B. Opt. Lett. 2012, 37, 2211–2213.
- [26] Mashiko, H.; Gilbertson, S.; Chini, M.; Feng, X.; Yun, C.; Wang, H.; Khan, S.D.; Chen, S.; Chang, Z. Opt. Lett. 2009, 34, 3337–3339.
- [27] Mashiko, H.; Bell, M.J.; Beck, A.R.; Abel, M.J.; Nagel, P.M.; Steiner, C.P.; Robinson, J.; Neumark, D.M.; Leone, S.R. Opt. Express 2010, 18, 25887–25895.
- [28] Gilbertson, S.; Khan, S.D.; Wu, Y.; Chini, M.; Chang, Z. Phys. Rev. Lett. 2010, 105, 093902.
- [29] Iaconis, C.; Walmsley, I.A. IEEE J. Quantum Electron. 1999, 35, 501–509.

- [30] Itatani, J.; Quéré, F.; Yudin, G.L.; Ivanov, M.Y.; Krausz, F.; Corkum, P.B. Phys. Rev. Lett. 2002, 88, 173903.
- [31] Quéré, F.; Mairesse, Y.; Itatani, J. J. Mod. Opt. **2005**, *52*, 339–360.
- [32] Gagnon, J.; Goulielmakis, E.; Yakovlev, V.S. Appl. Phys. B: Lasers Opt. 2008, 92, 25–32.
- [33] Kane, D.J. J. Opt. Soc. Am. B 2008, 25, A120-A131.
- [34] Loh, Z.-H.; Khalil, M.; Correa, R.E.; Leone, S.R. Rev. Sci. Instrum. 2008, 79, 073101.
- [35] Chan, W.F.; Cooper, G.; Brion, C.E. Phys. Rev. A: At., Mol., Opt. Phys. 1991, 44, 186–204.
- [36] Gaarde, M.B.; Buth, C.; Tate, J.L.; Schafer, K. J. Phys. Rev. A: At, Mol., Opt. Phys. 2011, 83, 013419.
- [37] Cohen-Tannoudji, C.; Dupont-Roc, J.; Grynberg, G. Atom-Photon Interactions; Wiley-VCH Verlag: Weinheim, 2004.
- [38] Liao, P.F.; Bjorkholm, J.E. Opt. Commun. 1976, 16, 392–395.
- [39] Drake, G. W. F. In Springer Handbook of Atomic, Molecular, and Optical Physics; Drake, G.W.F., Ed.; Springer: Berlin, 2006; Vol. 1, pp 199–219.